



AFRL-RX-WP-TP-2009-4127

**PATH FORCE CONTROL FOR FRICTION STIR
WELDING PROCESSES (PREPRINT)**

Xin Zhao, Prabhanjana Kalya, Robert G. Landers, and K. Krishnamurthy
University of Missouri-Rolla

FEBRUARY 2009

Approved for public release; distribution unlimited.

See additional restrictions described on inside pages

STINFO COPY

**AIR FORCE RESEARCH LABORATORY
MATERIALS AND MANUFACTURING DIRECTORATE
WRIGHT-PATTERSON AIR FORCE BASE, OH 45433-7750
AIR FORCE MATERIEL COMMAND
UNITED STATES AIR FORCE**

REPORT DOCUMENTATION PAGE				<i>Form Approved</i> OMB No. 0704-0188	
<small>The public reporting burden for this collection of information is estimated to average 1 hour per response, including the time for reviewing instructions, searching existing data sources, gathering and maintaining the data needed, and completing and reviewing the collection of information. Send comments regarding this burden estimate or any other aspect of this collection of information, including suggestions for reducing this burden, to Department of Defense, Washington Headquarters Services, Directorate for Information Operations and Reports (0704-0188), 1215 Jefferson Davis Highway, Suite 1204, Arlington, VA 22202-4302. Respondents should be aware that notwithstanding any other provision of law, no person shall be subject to any penalty for failing to comply with a collection of information if it does not display a currently valid OMB control number. PLEASE DO NOT RETURN YOUR FORM TO THE ABOVE ADDRESS.</small>					
1. REPORT DATE (DD-MM-YY) February 2009		2. REPORT TYPE Technical Paper Preprint		3. DATES COVERED (From - To)	
4. TITLE AND SUBTITLE PATH FORCE CONTROL FOR FRICTION STIR WELDING PROCESSES (PREPRINT)				5a. CONTRACT NUMBER FA8650-04-C-5704	
				5b. GRANT NUMBER	
				5c. PROGRAM ELEMENT NUMBER 78011F	
6. AUTHOR(S) Xin Zhao, Prabhanjana Kalya, Robert G. Landers, and K. Krishnamurthy				5d. PROJECT NUMBER 2865	
				5e. TASK NUMBER 25	
				5f. WORK UNIT NUMBER 25100000	
7. PERFORMING ORGANIZATION NAME(S) AND ADDRESS(ES) University of Missouri-Rolla Missouri University of Science and Technology Mechanical and Aerospace Engineering Department 400 W. 13th Street Rolla, MO 65409-0050				8. PERFORMING ORGANIZATION REPORT NUMBER	
9. SPONSORING/MONITORING AGENCY NAME(S) AND ADDRESS(ES) Air Force Research Laboratory Materials and Manufacturing Directorate Wright-Patterson Air Force Base, OH 45433-7750 Air Force Materiel Command United States Air Force				10. SPONSORING/MONITORING AGENCY ACRONYM(S) AFRL/RXLMP	
				11. SPONSORING/MONITORING AGENCY REPORT NUMBER(S) AFRL-RX-WP-TP-2009-4127	
12. DISTRIBUTION/AVAILABILITY STATEMENT Approved for public release; distribution unlimited.					
13. SUPPLEMENTARY NOTES PAO Case Number: 88 ABW-2008-1142; Clearance Date: 26 Nov 2008. Paper contains color.					
14. ABSTRACT In Friction Stir Welding (FSW) processes, force control can be used to achieve good welding quality. This paper presents the systematic design and implementation of a FSW path force controller. The path force is modeled as a nonlinear function of the FSW process parameters (i.e., plunge depth, tool traverse rate, and tool rotation speed). An equipment model, which includes a communication delay, is constructed to relate the commanded and measured tool rotation speed. Based on the dynamic process and equipment models, a feedback controller for the path force is designed using the Polynomial Pole Placement technique. The controller is implemented in a Smith Predictor-Corrector structure to compensate for the inherent equipment communication delay and the controller parameters are tuned to achieve the best closed loop response possible given equipment limitations. In the path force controller implementation, a constant path force is maintained, even in the presence of gaps, and wormhole generation during the welding process is eliminated by regulating the path force.					
15. SUBJECT TERMS friction stir welding (FSW), force control, path force, welding					
16. SECURITY CLASSIFICATION OF:			17. LIMITATION OF ABSTRACT: SAR	18. NUMBER OF PAGES 14	19a. NAME OF RESPONSIBLE PERSON (Monitor) Todd J. Turner 19b. TELEPHONE NUMBER (Include Area Code) N/A
a. REPORT Unclassified	b. ABSTRACT Unclassified	c. THIS PAGE Unclassified			

PATH FORCE CONTROL FOR FRICTION STIR WELDING PROCESSES

Xin Zhao, Prabhanjana Kalya, Robert G. Landers, and K. Krishnamurthy
Missouri University of Science and Technology
Mechanical and Aerospace Engineering Department
400 W. 13th Street, Rolla, Missouri 65409–0050
{xzvc8;pk34b;landersr;kkrishna}@mst.edu

ABSTRACT

In Friction Stir Welding (FSW) processes, force control can be used to achieve good welding quality. This paper presents the systematic design and implementation of a FSW path force controller. The path force is modeled as a nonlinear function of the FSW process parameters (i.e., plunge depth, tool traverse rate, and tool rotation speed). An equipment model, which includes a communication delay, is constructed to relate the commanded and measured tool rotation speed. Based on the dynamic process and equipment models, a feedback controller for the path force is designed using the Polynomial Pole Placement technique. The controller is implemented in a Smith Predictor–Corrector structure to compensate for the inherent equipment communication delay and the controller parameters are tuned to achieve the best closed loop response possible given equipment limitations. In the path force controller implementation, a constant path force is maintained, even in the presence of gaps, and wormhole generation during the welding process is eliminated by regulating the path force.

INTRODUCTION

Friction Stir Welding (FSW) is a new solid state welding technology that has been used successfully in many joining applications. In FSW processes, a rotating non-consumable tool, consisting of a pin and shoulder, plunges into the part such that both the pin and shoulder are in contact with the part. The tool rotation induces gross material plastic deformation due to an elevated temperature field. The tool travels along, or across, the intersection of two parts after dwelling for a specified amount of time, and joins the parts as the tool leaves the processing zone. This technique has advantages in that it can join materials that are difficult to weld by conventional welding processes, such as 2000 and 7000 series aluminum alloys, and part distortion and residual stresses are low. The FSW process is also environmentally friendly since harmful gases are not generated during the process.

It is often desirable to regulate the forces that are produced in FSW processes since machine geometric errors, structural deflections, improper fixturing, changes in thermal boundary conditions, etc. can cause poor weld quality, such as internal and surface voids, if constant process parameters are utilized. Experimental results [1] revealed a relationship between the generation of void defects and the path force: when the path force is above a critical value, void defects are generated. This result suggests that a feedback path force controller can be designed to eliminate the generation of void defects during FSW processes.

Many manufacturing operations may be improved by regulating the process forces (e.g., [2–6]); however, force control has not been extensively investigated in the open literature. Smith [7] presented illustrations of robotic FSW with a serial industrial robot IRB 7600 working in a force feedback control mode. Strombeck [8] gave welding examples using the parallel industrial robot RIFTEC 600 with force feedback control. Cook [9] investigated the relationship between the increment in plunge depth and the corresponding increment in the axial force and noted that a force controller stability problem could be caused by the transient response characteristics during the beginning welding stage. Most current axial force feedback control algorithms in FSW machines are proprietary and, to the author's knowledge, no systematic design techniques are available in the literature.

The rest of this paper is organized as follows. First, equipment utilized in this study and noise filtering are described. Dynamic FSW process models for the path force and the equipment dynamic model for the tool rotation speed, which will be adjusted to maintain a constant path force, are presented. Then, the detailed design procedure of the force controller using the Polynomial Pole Placement method implemented in a Smith Predictor–Corrector structure is introduced. Lastly, experimental validation studies are conducted and discussed.

Most force controllers for FSW processes regulate the axial force and systematic design methodologies are lacking. This paper makes contributions in that 1) a methodology that accounts for communication delays and the nonlinear static behavior between the force and tool rotation speed is presented and 2) the path force (i.e., the force in the direction of tool motion) is regulated. It will be seen that wormholes can be eliminated by regulating the path force.

EXPERIMENTAL PLATFORM

The FSW system (Figure 1) used to conduct the experiments in this paper consists of a six degree of freedom robot (ABB IRB 940 Tricept robot), a FSW spindle head, a six axis force/moment sensor, and an open architecture control system. The robot has three non parallel telescopic translational joints and three rotational joints, and is retrofitted with a FSW spindle head to provide the rotational tool motion. The FSW spindle head (Figure 2) has a rotational axis driven by a 10 hp Exlar SLM115-368 servo motor with a rotational speed range of ± 3000 rpm. The load capability of the spindle is 9.0 kN along the tool axis and 4.5 kN in the radial direction. The six-axis force/moment sensor system (JR3 Inc. model 75E20S-M125A-A 6000N1150) provides measurements of the process loading: the forces in three orthogonal directions and moments about each direction. The output analog voltage signal ranges are ± 10.0 V. The rated sensor forces are 6 kN in the x and y-directions and 12 kN in the z-direction. The rated moments are 1,150 N-m about all three directions. The teach pendant is used to manually control and program the robot.

The IRB 940 Tricept robot uses an S4cPlus robot control unit with RAPID as the programming language. The high level language RAPID enables the operator to pre-program the processing sequence and control algorithms in simple text formats, upload the source programs to the control unit, and compile and execute the code. Figure 3 illustrates the basic structure and functional blocks of the program used for the experiments conducted in this paper. The program consists of the initialization routines, a main welding loop executing in real-time during the welding process, and data storage routines executed after the process is complete. An interrupt procedure with an interval of 0.1 s is triggered to provide a constant frequency of data acquisition and process parameter outputs as soon as the main welding loop is entered. During the interrupt procedure, the sensor data (i.e., forces and measured process parameters) are collected and the output signals (i.e., commanded process parameters) are calculated. These output signals are sent to their respective amplifiers during the main welding loop and, after the main loop finishes, all collected sensor data are saved to the control unit hard disk.

The tool is threaded, contains three flats, and has a scrolled shoulder. All experiments are conducted with zero tilt angle. The force signal is filtered in hardware via a low pass filter.

The experimental data contains significant electrical noise. Therefore, a five-point moving average was empirically determined to provide good data filtering without significant

signal delay and unduely taxing the system's limited computational bandwidth. After implementing the filter, the standard deviation of the steady state force data with constant process parameters decreases approximately 50%.

PROCESS AND EQUIPMENT DYNAMIC MODELING

There has been a substantial amount of work in detailed thermo-mechanical models for FSW processes [10–12]. However, these models are solved using finite difference or finite element techniques and the computational requirements limit their use for controller design and implementation. In this paper, the controller designs are based on empirical dynamic models of the FSW process for 6061-T6 aluminum alloy (composition by weight: 97.9% Al, 0.60% Si, 0.30% Cu, 1.0% Mg, and 0.20% Cr). Based on the work of Zhao *et al.* [13], the path (F_p) force model is developed using the Least Square and Recursive Least Square techniques. Note this model considers the filtered force, not the raw force signal. The model is a first order system with tool rotation speed as the input process parameter. Other factors can be treated as disturbances (e.g., fixturing) or are constant during the operation (e.g., material properties, tool geometry, travel and work angles). Given a sampling frequency of 10 Hz, the model is converted into the discrete time domain with a Zero-Order-Hold transformation

$$F_p(z) = \frac{2.20 \cdot 10^{-2} v^{0.999}}{z - 0.854} \omega^{-1.23}(z) \quad (1)$$

where F_p is the path force and ω is the tool rotation speed. Due to the dynamic characteristics of the actuators and the communication delays that exist between the processors handling the high and low level computations, a dynamic relationship exists between the commanded and measured tool rotation speed. Given the nonlinear relationships between the path force and tool rotation speed, as shown in equation (1) the dynamic relationships between $\omega^{-1.23}$ and $\omega_c^{-1.23}$ are modeled,

where ω_c is the commanded tool rotation speed. Step change experiments in the tool rotation speed are conducted to determine the relationship. Experimental results show this relationship can be described by a pure delay and a first order transient response. Figure 4 shows experimental results for the tool rotation speed for step changes in the commanded tool rotation speed. The number of delay periods are visually observed and the model time constants and gains are estimated by the Recursive Least Square method. Nine runs are conducted and, therefore, 36 transient response data sets are collected. Delay times and time constants for the tool rotation speed equipment model are shown in Figure 5. The gain is unity.

Taking the average delay times and time constants, the dynamic relationship between the commanded and measured tool rotation speed is

$$\frac{\omega^{-1.23}(s)}{\omega_c^{-1.23}(s)} = \frac{e^{-0.294s}}{0.114s+1} \quad (2)$$

The standard deviation of the tool rotation speed delay times is $6.30 \cdot 10^{-2}$ s and the standard deviation of the tool rotation speed time constants is $5.59 \cdot 10^{-2}$ s. Since the welding program operates at a sampling frequency of $f_s = 10$ Hz, the number of delay periods can be calculated based on the average equipment model delay time T_d and f_s as $n = \text{round}(T_d/f_s)$. Thus, the tool rotation speed equipment model, using a Zero–Order–Hold transformation, is

$$\frac{\omega^{-1.23}(z)}{\omega_c^{-1.23}(z)} = \frac{0.587}{z-0.413} z^{-3} \quad (3)$$

A series of sinusoidal experiments are conducted to validate the tool rotational speed equipment model. The commanded tool rotation speed is $\omega_c = 1900 + 300\sin(2\pi f_{\omega} t)$. The frequencies of the sinusoidal experiments are limited by the rate limits imposed on the tool rotation speed, which is empirically determined and is 1000 rpm/s. Therefore, the maximum frequencies for the tool rotation speed sinusoidal experiments is 0.531 Hz. Four frequencies are selected within this range. The model Bode Diagrams and the measured magnitude ratios and phase shifts are shown in Figure 6.

The Bode Diagrams indicate the models fit the experimental results very well. The maximum differences between the tool rotation speed modeled and measured magnitudes and phase shifts are 0.403 dB and 12.0°, respectively. The differences are due to the fact that the delay times in the discrete time models are rounded to integers based on the sampling rate.

CONTROLLER DESIGN

In this section feedback controllers utilizing the Polynomial Pole Placement (PPP) technique are designed to regulate the path force at a constant value. The controller is implemented in a Smith Predictor–Corrector (SPC) structure to compensate for the inherent equipment communication delay. The controller closed loop system block diagram is shown in Figure 7. The parameter F_r is the reference force, F is the measured force, E is the error between the reference and measured forces, U is the control signal, C is the controller transfer function, G is the model force process transfer function, and n is the number of equipment delay periods.

Since the sampling rate is $f_s = 10$ Hz, the operating bandwidth is 0–5 Hz. The design procedure consists of the following steps:

1. Calculate process model's zeros and poles.
2. Select closed loop system poles based on results of Step 1.
3. Calculate controller transfer function using the PPP technique with Internal Model Principle (IMP) based on closed loop poles selected in Step 2.

4. Evaluate closed loop system's stability and robustness within operating bandwidth using stability margins and sensitivity function.

The above design procedure is iterative, and Steps 2–4 may need to be repeated according to the stability and robustness results and experimental investigations.

The path force controller is designed using the PPP technique with the application of the IMP. The plant transfer function $G_0(z)$, incorporating the path force process model in equation (1) and the rotational speed model in equation (3), is

$$G_0(z) = G(z) z^{-3} \quad (4)$$

where

$$G(z) = \frac{b(z)}{a(z)} = \frac{1.29 \cdot 10^{-2} v^{0.999}}{z^2 - 1.27z + 0.353} \quad (5)$$

The poles are located at 0.854 and 0.413. The first pole is due to the path force process model dynamics and the second pole is due to the equipment model dynamics. The operating bandwidth is again 5 Hz.

The order of the path force dynamic model is 2; therefore, the order of the closed loop characteristic polynomial is 4. The closed loop characteristic polynomial is manipulated to contain the factors of $a(z)$ so that the order of the closed loop transfer function is reduced. An initial design of $\alpha(z)$ is

$$\alpha(z) = (z - r_0)(z - r_1)(z - r_2)z \quad (6)$$

where r_0 is the dominant pole and r_1 and r_2 are identical to the plant transfer function poles. The time constant of the dominant pole is set to 1.2 s, based on experimental results, so that the closed loop system response is fast and the system still has sufficient stability and robustness. Therefore, $r_0 = 0.926$. Substituting r_0 , r_1 , and r_2 into equation (6)

$$\alpha(z) = z^4 - 2.19z^3 + 1.52z^2 - 0.324z \quad (7)$$

The controller transfer function is

$$C(z) = \frac{p(z)}{q(z)} = \frac{(6.19z^2 - 7.84z + 2.18)v^{-0.999}}{z^2 - 0.920z - 8.00 \cdot 10^{-2}} \quad (8)$$

The controller is an explicit function of v and, therefore, inherently compensates for variations in the tool traverse rate. The closed loop design is also evaluated by computing the sensitivity function and stability margins. Figure 8 shows the value of sensitivity function in the range of $0 < f < 5$ Hz, and the maximum value is 1.10. Figure 9 shows the Bode Diagram, including the stability margins. The magnitude and phase margins are 22.6 dB and 83.9°, respectively. Therefore, the requirements for both sensitivity and stability margins are

satisfied.

The path force controller is implemented in a Smith Predictor–Corrector structure and the control law is

$$\begin{aligned} u(k) = & 0.920u(k-1) + 8.00 \cdot 10^{-2}u(k-2) \\ & + 6.19v^{-0.999} [e(k) - e_1(k)] \\ & - 7.84v^{-0.999} [e(k-1) - e_1(k-1)] \\ & + 2.18v^{-0.999} [e(k-2) - e_1(k-2)] \end{aligned} \quad (9)$$

where

$$\begin{aligned} e_1(k) = & 1.27e_1(k-1) - 0.355e_1(k-2) \\ & + 1.29v^{0.999} [u(k-2) - u(k-5)] \end{aligned} \quad (10)$$

and $u(k) = \omega_c^{-1.23}(k)$ is the control signal. The commanded tool rotation speed is determined using the nonlinear mapping $\omega_c(k) = u^{1.23}(k)$.

EXPERIMENTAL VALIDATION

In this section, lap welding experiments are conducted to validate the performances of the path force controller.

In the first set of path force controller validation experiments, the controller is implemented to track constant reference path forces and the plunge depth and tool traverse rate are constant. In these experiments, the sheets are lap welded, as shown in Figure 10. According to the path force model, the plunge depth does not affect the force significantly; therefore, a plunge depth of 4.20 mm is selected, based upon experimental observations, to ensure the tool shoulder maintains contact with the plate and surface voids are not created during the welding process. Three experiments are conducted with different traverse rates and reference force levels such that the shoulder maintains contact with the plate and good weld quality is obtained (i.e., surface voids are not created). The reference path force changes from the high (F_{r1}) to the low (F_{r2}) value in a step-wise manner in the middle of the weld. Figure 11 shows the experimental results for the second test and Table 1 shows the process parameters and the path force averages and standard deviations during the two steady-state portions for each test. The results show the controller tracks the reference path force well for all three tests.

The second set of path force validation experiments is designed to examine the controller's performance when welding along skin-to-skin gaps. The experimental setup is shown in Figure 12. In this setup, sheets are both lap and butt welded. Four gap sizes are examined: a constant gap of 0.381 mm, a constant gap of 0.762 mm, a tapered gap increasing linearly from 0.381 to 0.762 mm, and no gap. The reference path force experiences a step-wise change from F_{r1} to F_{r2} in the

middle of the weld. A constant traverse rate of 3.2 mm/s, for which the path force has the smallest standard deviation when tracking the lowest force, is applied for all three experiments. Due to the gap, a constant plunge depth of 4.25 mm, 0.05 mm deeper as compared to the experiments without gaps, is applied to obtain the same path force level. Figure 13 shows the experimental results for test 3 and Table 2 shows the tracking performance for each test. The results show that the steady-state averages and standard deviations are similar to those obtained in test 3 of the first set of experiments, which has the same traverse rate and reference force. This indicates the path force controller also works well when welding along skin-to-skin gaps and the path force is not significantly affected by the presence of these types of gaps.

The third set of experiments is designed to demonstrate the ability of the path force controller to eliminate the generation of wormholes during the welding process. In this experiment, the plunge depth and traverse rate are 4.20 mm and 3.20 mm/s, respectively, and the initial tool rotation speed is 900 rpm. The sheets are butt welded, as shown in Figure 10. During the first 20 seconds, the controller is not implemented and after 20 seconds, the controller is activated to regulate the path force at a reference value of 0.22 kN. The reference path force is selected so a good weld will be obtained without wormholes or the creation of surface voids. The experimental results are shown in Figure 14. It is observed that the implementation of the controller maintained the path force at a constant value. In the steady state with force control (5.0–20.0 s), the average value of path force is 0.215 kN and the standard deviation is $7.95 \cdot 10^{-3}$ kN. Figure 15 shows pictures of the weld cross-sections during the steady-states both with path force control (26.5–48.0 s) and with constant tool rotation speed (20.0–48.0 s). It is observed that with the implementation of the path force controller, void defects, as shown in subplot (b), are eliminated, as shown in subplot (a).

SUMMARY AND CONCLUSIONS

A model-based, path force controller was designed using the Polynomial Pole Placement technique with the Internal Model Principle for friction stir welding processes. The model consisted of an equipment model, which was developed in this paper, and a process model, that was taken from the literature. The controller was implemented in a Smith Predictor–Corrector structure to compensate for inherent equipment communication delays. A detailed design procedure was introduced and several experiments were conducted to validate the controller's performance.

Experimental results validated the developed equipment model. The path force controller was experimentally shown to be able to track a constant path, even when gaps were encountered along the weld path. One experiment showed that the wormhole defect during the welding process can be eliminated by the implementation of the path force controller.

As seen in Figure 5, there is slight variation in the

communication delay. To improve the performance shown in this paper, a variable delay time control scheme would need to be implemented.

ACKNOWLEDGEMENT

The authors wish to acknowledge the financial support for this work from the Missouri University of Science and Technology's Center for Aerospace Manufacturing Technologies (Air Force Research Laboratory contract FA8650-04-C-5704) and the technical support of colleagues at Missouri S&T, the Boeing Company, and the Air Force Research Laboratory.

REFERENCES

[1] Kalya, P., 2007, *Modeling and Control of Friction Stir Welding*, Doctoral Dissertation, University of Missouri-Rolla, Department of Mechanical and Aerospace Engineering, Rolla, Missouri.

[2] Chen, L., Stango, R.J., and Cariapa, V., 2001, "A Force-Control Model for Edge-Deburring with Filamentary Brush," *ASME Journal of Manufacturing Science and Engineering*, Vol. 123, No. 3, pp. 528-532.

[3] Viswanathan, V., Kinsey, B., and Cao, J., 2003, "Experimental Implementation of Neural Network Springback Control for Sheet Metal Forming," *ASME Journal of Engineering Materials and Technology*, Vol. 125, No. 2, pp. 141-147.

[4] Liang, S.Y., Hecker, R.L., and Landers, R.G., 2004, "Machining Process Monitoring and Control: The State-of-the-Art," *ASME Journal of Manufacturing Science and Engineering*, Vol. 126, No. 2, pp. 297-310.

[5] Xu, C. and Shin, Y.C., 2007, "Control of Cutting Force for Creep-Feed Grinding Processes using a Multi-Level Fuzzy Controller," *ASME Journal of Dynamic Systems, Measurement, and Control*, Vol. 129, No. 4, pp. 480-492.

[6] Mason, M.S., Huang, T., Landers, R.G., Leu, M.C., and Hilmas, G.E., 2006, "Freeform Extrusion of High Solids Loading Ceramic Slurries, Part II: Extrusion Process Control," *Seventeenth Annual Solid Freeform Fabrication Symposium*, Austin, Texas, August 14-16.

[7] Smith, C.B., Hinrichs, J.F., and Crusan, W.A., 2003, "Robotic Friction Stir Welding: the State of the Art," *Proceedings of the 4th International Symposium of Friction Stir Welding*, Park City, Utah, May 14-16.

[8] Von Strombeck, A., Schilling, C., and Dos Santos, J.F., 2000, "Robotic Friction Stir Welding - Tool, Technology and Applications," *Proceedings of the 2nd International Symposium of Friction Stir Welding*, Gothenburg, Sweden, June 26-28.

[9] Cook, G.E., Smart, H.B., Mitchell, J.E., Strauss, A.M., and Crawford, R., 2003, "Controlling Robotic Friction Stir Welding," *Welding Journal*, Vol. 82, No. 6, pp. 28-34.

[10] Chao, Y.J., Qi, X., and Tang, W., 2003, "Heat Transfer in Friction Stir Welding - Experimental and Numerical Studies," Vol. 125, No. 1, pp. 138-145.

[11] Ulysse, P., 2002, "Three-Dimensional Modeling of the Friction Stir Welding Process," *International Journal of*

Machine Tools and Manufacture, Vol. 42, No. 14, pp. 1549-1557.

[12] Heurtier, P., Jones, M., Desrayaud, C., Driver, J., Montheillet, F., and Allehaux, D., 2006, "Mechanical and Thermal Modeling of Friction Stir Welding," *Journal of Materials Processing Technology*, Vol. 171, No. 3, pp. 348-357.

[13] Zhao, X., Kalya, P., Landers, R.G., and Krishnamurthy, K., 2007, "Empirical Dynamic Modeling of Friction Stir Welding Processes," *ASME International Conference on Manufacturing Science and Engineering*, Atlanta, Georgia, October 15-18.

[14] Åström, K.J. and Wittenmark, B., 1997, *Computer-Controlled Systems-Theory and Design*, 3rd ed., pp. 110-111 and 183-185, Prentice Hall, Upper Saddle River, New Jersey.

[15] De Silva, C.W., 2004, *Mechatronics-An Integrated Approach*, pp. 1032-1034, CRC Press LLC, Boca Raton, Florida.

[16] Ogata, K., 2002, *Modern Control Engineering*, 4th ed., Prentice Hall, Upper Saddle River, New Jersey.

Table 1: Path Force Controller Tracking Performance during Steady-State ($d = 4.20$ mm). F_{1ss} and F_{2ss} are Steady-State Path Forces for First and Second, respectively, Sections.

Test	1	2	3
v (mm/s)	2.0	2.6	3.2
F_{r1} (kN)	0.16	0.19	0.23
F_{r1ss} (kN)	0.159	0.191	0.236
$\sigma(F_1)$ (kN)	$1.29 \cdot 10^{-2}$	$1.18 \cdot 10^{-2}$	$1.34 \cdot 10^{-2}$
F_{r2} (kN)	0.13	0.16	0.20
F_{r2ss} (kN)	0.131	0.162	0.202
$\sigma(F_2)$ (kN)	$0.727 \cdot 10^{-2}$	$0.601 \cdot 10^{-2}$	$0.592 \cdot 10^{-2}$

Table 2: Tracking Performance of Path Force Controller when Welding along Gaps ($d = 4.25$ mm and $v = 3.2$ mm/s). The Parameters F_{1ss} and F_{2ss} are Steady-State Path Forces for First and Second, respectively, Sections.

Test	1	2	3	4
g (mm)	0.381	0.762	0.381→0.762	0
F_{r1} (kN)	0.23	0.23	0.23	0.23
F_{r1ss} (kN)	0.232	0.228	0.237	0.230
$\sigma(F_1)$ (kN)	7.37e-3	8.36e-3	1.06e-2	8.61e-3
F_{r2} (kN)	0.20	0.20	0.20	0.20
F_{r2ss} (kN)	0.200	0.201	0.204	0.202
$\sigma(F_2)$ (kN)	8.38e-3	6.44e-3	6.36e-3	6.63e-3

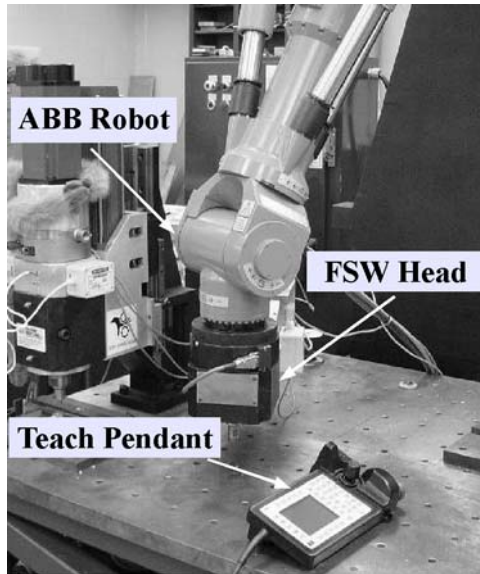


Figure 1: Friction Stir Welding System.

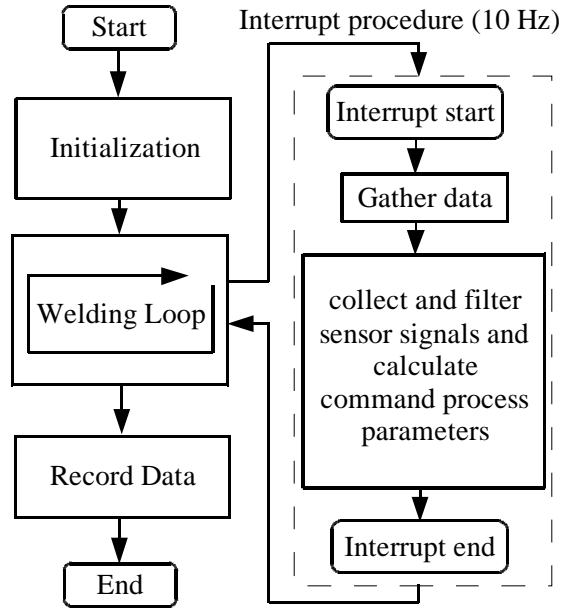


Figure 3: Robotic Friction Stir Welding Force Control Program Functional Block Structure.

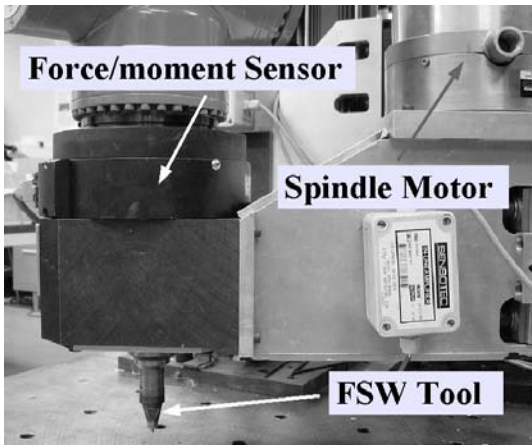


Figure 2: FSW Head with Tool and Six-Axis Force/Moment Sensor.

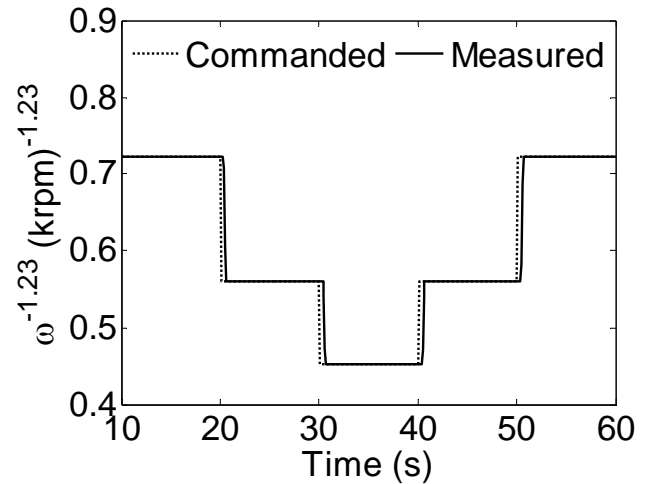


Figure 4: Commanded and Measured Tool Rotation Speed Responses.

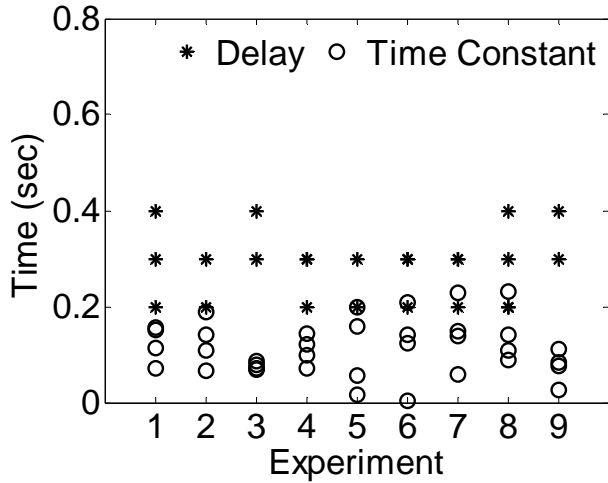


Figure 5: Tool Rotation Speed Equipment Model Delays and Time Constants.

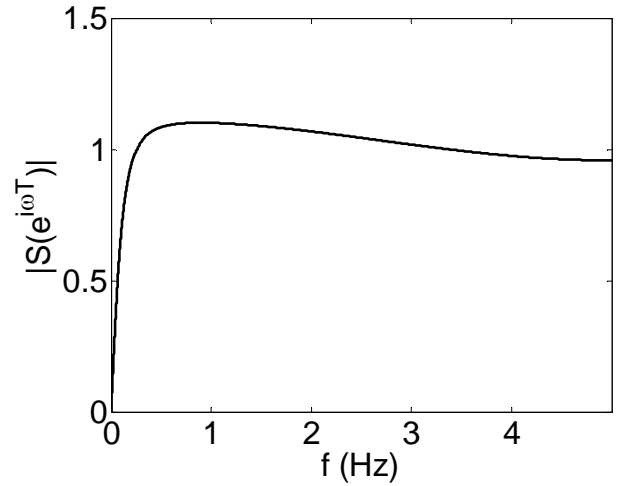


Figure 8: Path Force Closed Loop System Sensitivity Functions.

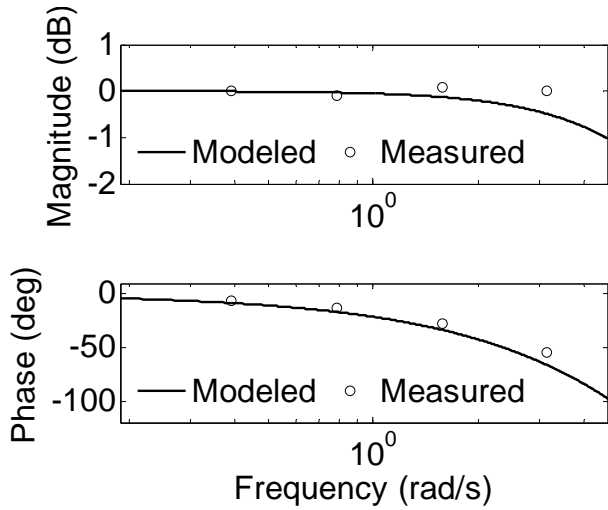


Figure 6: Tool Rotation Speed Equipment Modeled and Measured Bode Diagrams.

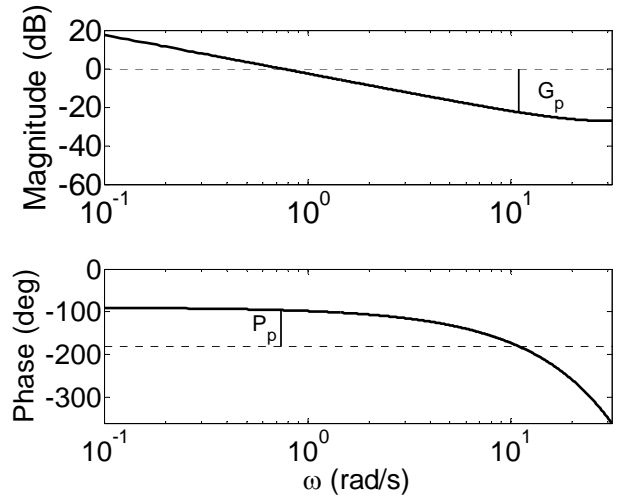


Figure 9: Path Force Control System Bode Diagrams and Stability Margins ($G_p = 22.6$ dB and $P_p = 83.9^\circ$).

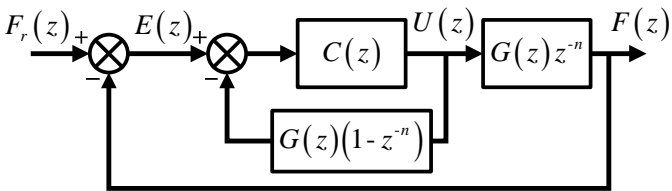


Figure 7: Closed Loop Force Control System Block Diagram.

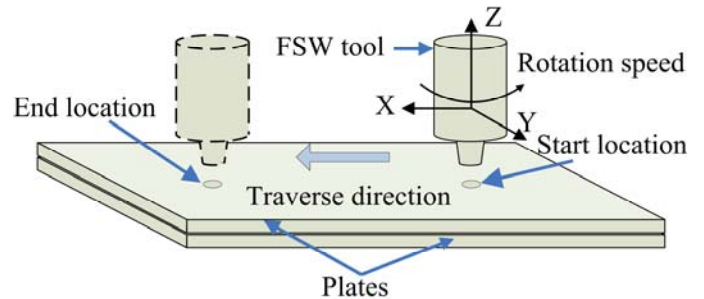


Figure 10: Lap Welding Experimental Setup.

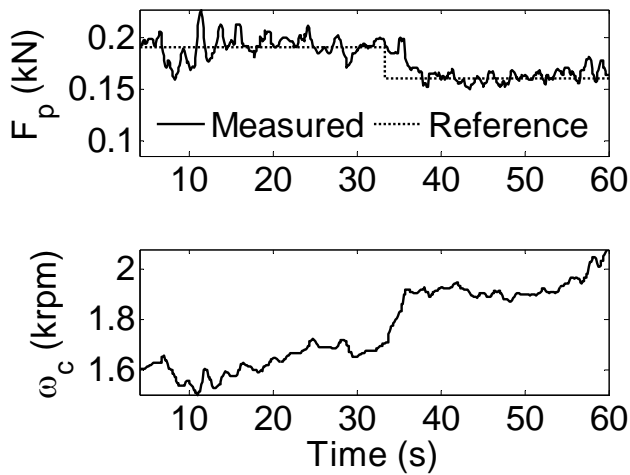


Figure 11: Path Force and Tool Rotation Speed for Path Force Controller ($d = 4.20 \text{ mm}$ and $v = 2.6 \text{ mm/s}$).

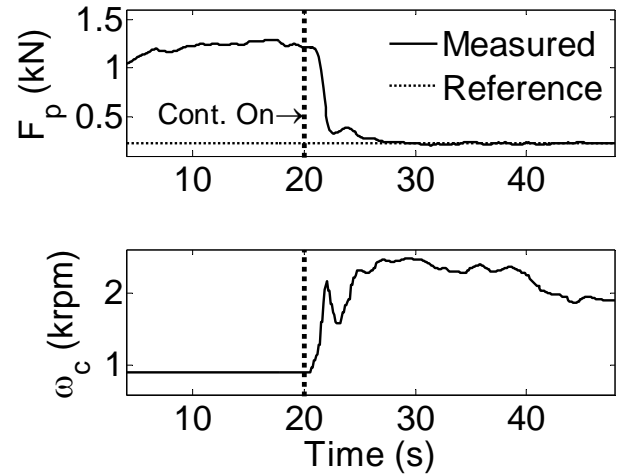


Figure 14: Path Force before and after Path Controller Implementation ($d = 4.20 \text{ mm}$, $v = 3.2 \text{ mm/s}$, and $F_r = 0.22 \text{ kN}$).

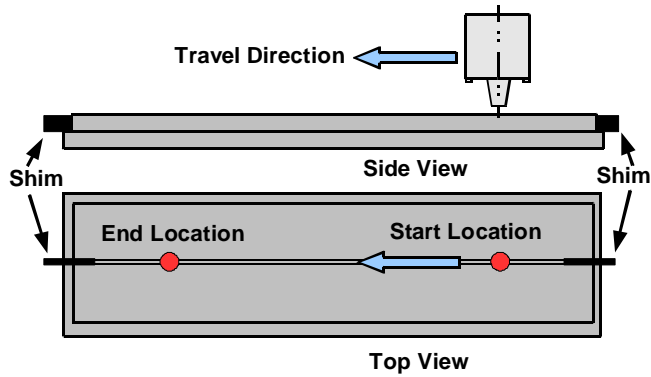


Figure 12: Experimental Setup for Welding Experiments along a Gap.

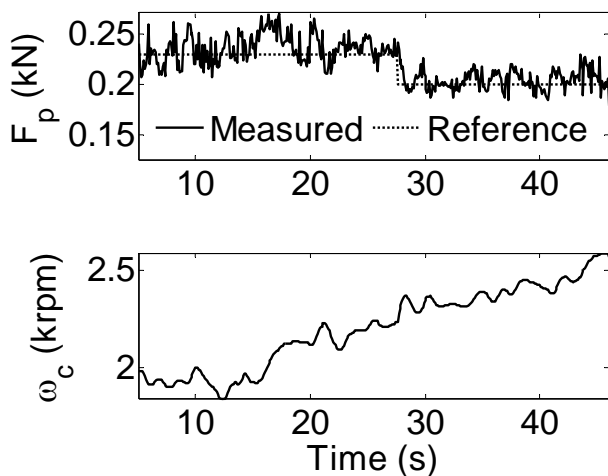


Figure 13: Path Force and Tool Rotation Speed when Welding along a Gap with Implementation of Path Force Controller ($d = 4.25 \text{ mm}$, $v = 3.2 \text{ mm/s}$, and tapered gap, $g = 0.381 \rightarrow 0.762 \text{ mm}$).

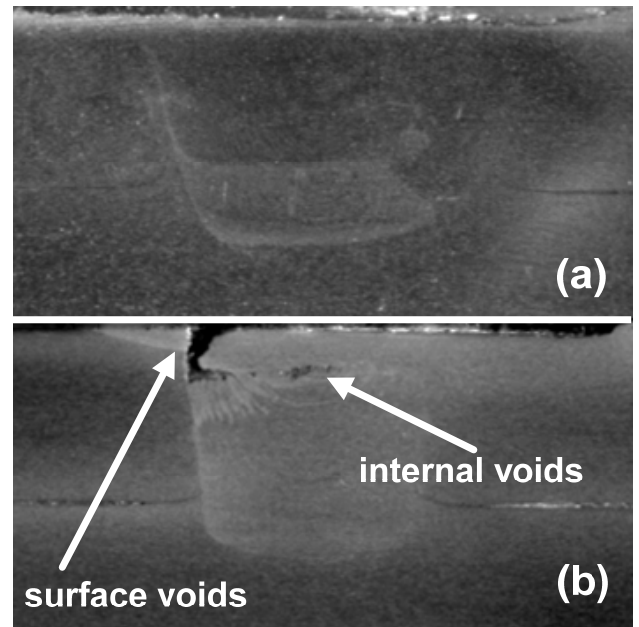


Figure 15: Nugget Cross Sections (a) with Path Force Control ($d = 4.20 \text{ mm}$, $v = 3.2 \text{ mm/s}$, and $F_r = 0.22 \text{ kN}$) and (b) without Path Force Control ($d = 4.20 \text{ mm}$, $v = 3.2 \text{ mm/s}$, and $\omega = 900 \text{ rpm}$).